arXiv:2407.18245v2 [cs.CV] 5 Dec 2024

VGGHeads: 3D Multi Head Alignment with a Large-Scale Synthetic Dataset

Orest Kupyn[1,2] Eugene Khvedchenia[3] Christian Rupprecht[1]

[1] University of Oxford [2] Piñata Farms, Los Angeles, USA [3] Ukrainian Catholic University

Figure 1. **VGGHeads** Top: Our fully synthetic large-scale dataset for 3D Multi Head Alignment with a wide variety of scenes, numbers of people, and rich annotations for every human head. Bottom: The model trained on this fully synthetic data generalizes to in-the-wild scenes.

Abstract

Human head detection, keypoint estimation, and 3D head model fitting are essential tasks with many applications. However, traditional real-world datasets often suffer from bias, privacy, and ethical concerns, and they have been recorded in laboratory environments, which makes it difficult for trained models to generalize. Here, we introduce VGGHeads— a large-scale synthetic dataset generated with diffusion models for human head detection and 3D mesh estimation. Our dataset comprises over 1 million high-resolution images, each annotated with detailed 3D head meshes, facial landmarks, and bounding boxes. Using this dataset, we introduce a new model architecture capable of simultaneous head detection and head mesh reconstruction from a single image in a single step. Through extensive experimental evaluations, we demonstrate that models trained on our synthetic data achieve strong performance on real images. Furthermore, the versatility of our dataset makes it applicable across a broad spectrum of tasks, offering a general and comprehensive representation of human heads. The dataset, code, and model are available here.

1. Introduction

In recent years, the demand for high-quality datasets has surged across various domains of computer vision, particularly for tasks involving human head representation. Accurate head modeling is crucial for applications ranging from facial recognition [11] and animation [65] to augmented reality and medical imaging. Traditional datasets often fall short, either focusing narrowly on specific aspects like facial landmarks [76] or offering limited resolution and annotation types. Historically, head processing typically begins with face detection, followed by landmark detection in each detected face box. However, face bounding box detection, while useful for certain applications, does not generalize well to 3D reconstruction tasks. This is because bounding box methods typically operate on a limited range of poses, failing to capture the full variability and complexity of head orientations and structures needed for accurate 3D modeling. Moreover, real-world datasets come with significant challenges related to privacy, ethics, and consent, making it difficult to compile and use such data without legal and ethical concerns. For example, some well-established benchmarks, such as MS-Celeb [20] have been withdrawn due to licensing issues. A realistic synthetic head dataset can help

mitigate ethical and privacy risks.

In this work, we address the main bottleneck in human head modeling research by constructing a large-scale, diverse dataset with the help of image generative models in the form of latent diffusion models. Combined with the pseudo ground truth 3D morphable model (3DMM) head parameters, the dataset presents a general human head representation that includes 3D head pose and shape, expression, head and face bounding boxes, and 2D facial landmarks. We demonstrate that conditioning the generation on 2D body skeletons extracted from a large dataset of real images is sufficient to model a wide variety of in-the-wild scenes while also removing all private pixel information. Our contributions are as follows:

Large-Scale Synthetic Dataset: We present a large-scale synthetic dataset of over 1 million images, with each head in an image annotated with a detailed 3D head mesh. The detailed representation enables a wide range of downstream tasks, from face detection to 3D alignment, while the unprecedented scale ensures robust model training across diverse scenarios. Our experiments validate the quality, accuracy, and real-world generalization of our synthetic dataset.

Novel Model: We introduce a novel architecture and model trained on this dataset, capable of reconstructing multi-head meshes from a single input image. This model leverages the rich annotations in our dataset to simultaneously optimize bounding boxes, 3D vertices, rotations, and 2D landmarks to achieve robust and accurate reconstructions.

Generalized Representation: We conduct an extensive experimental evaluation to demonstrate the accuracy and effectiveness of our dataset and model. Firstly, we show that models trained on data from diffusion models achieve strong performance on real images, indicating the generalizability of our synthetic dataset. The model trained on our data recovers a general head representation that is applicable to multiple downstream tasks. We illustrate this versatility by applying the model to a wide range of tasks. The model trained on our dataset achieves comparable or superior performance to state-of-the-art methods in 3D Head Pose Estimation, 3D Mesh Estimation, Face and Head Detection, Head Alignment, and others.

2. Related Work

Head Detection: The simplest way to represent a head is with a face bounding box. Initially, face detectors used hand-crafted features [9, 57]. However, the rise of deep learning, particularly its effectiveness in enhancing object detection accuracy [50], has significantly reshaped the field. Current methodologies can be broadly categorized based on their utilization of region proposal networks into single-stage [27, 37] and two-stage methods [50]. Single-stage approaches, such as S^3FD [71], or PyramidBox [55], introduce a framework to detect smaller facial structures efficiently. Two-stage methodologies, based on Faster R-CNN [50] and R-FCN [8], integrate multi-scale techniques and novel pooling strategies to enhance detection performance [59, 68]. These approaches are, however, limited to detecting only a facial area and are not robust on side and out-of-distribution poses.

HollywoodHeads [58] extends the task to full head detection, releasing a dataset with movie scenes and a method to detect the human head across various poses. Similarly, SCUT-Head [47] introduces a dataset for head detection of 4405 images sampled from videos of classrooms and a cascade single-stage detection model. Yet, both datasets are limited to specific scenes, not reflecting a real-world distribution.

Recently, RetinaFace [12] improved detection accuracy by proposing multi-task learning of bounding box and facial landmarks, making a first step towards predicting a more general head representation. img2pose [3] directly regress 6DoF face pose, recovering both face bounding box and 3D head pose with a small set of parameters. Still, these methods only extend the detection task to predicting head pose or a small set of facial landmarks, which might not be sufficient for a wide range of head modeling methods.

3D Morphable Model: Early 3D Morphable Face Models (3DMM) provided a general purpose head representation [4]. A 3DMM is a statistical model of 3D facial shapes and textures built from scanned faces, allowing realistic 3D facial models to be created and manipulated with a few parameters. The Basel Face Model (BFM) [46] uses matrix decomposition to represent faces with parameters derived from 200 scans. More recent models, such as FLAME [33], cover the full 3D head mesh and are trained on a much larger dataset of scans.

Recently, several methods have addressed regressing 3DMM parameters from head crops. RingNet [53] estimates 3D face shape from a single image without direct 3D supervision, tackling the lack of ground truth data. 3DDFA [18] uses a Cascaded CNN to predict a dense 3DMM from a facial image, while 3DDFA-v2 [19] improves this with meta-joint optimization. DAD-3DHeads [43] introduces the first 3D head dataset in the wild and a model for 3D FLAME mesh reconstruction with direct 3D supervision. DECA [17], EMOCA [10] and MICA [77] address finer 3D head geometry modeling yet it still relies on robust coarse head detection and alignment methods in orders to extract high quality consistent crops from real world images.

Although these methods predict rich head representations, they require tightly cropped head images and can be computationally expensive, especially when applied serially. RetinaFace [12] is the first to recover 3D Facial Landmark in an end-to-end manner. Yet, the method is limited to the facial area only and utilizes only 5 ground-truth 2D facial landmarks to generate pseudo ground-truth 3D information, lack-

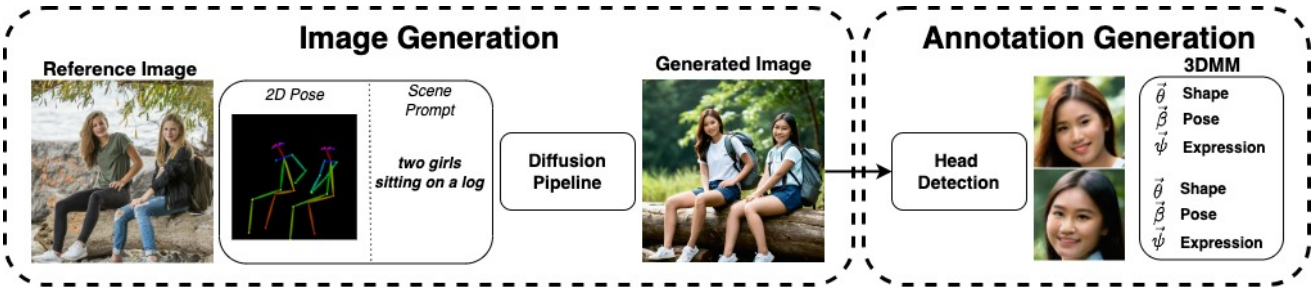

Figure 2. **Data Generation.** The predicted 2D body pose [2] and scene description [32] condition the image generation process. Binary detection model predicts head bounding boxes and 3DMM regressor [43] generates final annotation for each head crop.

ing consistency on hard samples. PIXIE [16] and PyMAF-X [69] make a step towards reconstructing head and full body models jointly. The methods still model only a limited set of parameters, lack the robustness on out od distribution poses and largely rely on coarse separate predictions.

The lack of large-scale datasets for direct head mesh regression in the wild and the complexity of the task due to the high-dimensional representation limits the progress in head modeling. VGGHeads efficiently addresses these issues by introducing a large-scale synthetic dataset with dense 3D head annotations and, to the best of our knowledge, the first model to directly recover multi-person head meshes from an image.

Synthetic Data Generation: Early synthetic data generation methods used 3D rendering engines to address 2D vision problems. Still, these approaches were constrained by the domain of 3D models and required modifications for each dataset and subtask. For example, Virtual KITTI [5] is limited to street driving scenes. More recent methods using generative adversarial networks (GANs) [64] offer greater flexibility and generalization to real-world images. However, these approaches primarily sample from the original dataset distribution, limiting their ability to incorporate new information. Recent methods based on diffusion models such as Diffumask [63] and DatasetDM [62] generate synthetic images and annotations for tasks such as semantic segmentation and depth prediction. Instance Augmentation [29] generate separate objects in an image, providing a framework to augment and anonymize datasets. However, these methods still require fine-tuning for specific datasets and have limited application to tasks with a low amount of ground truth data.

Synthetic Face Data: The synthetic face generation methods typically utilize rendering engines. Fake It Till You Make It [60] releases the first large-scale synthetic dataset combining a procedurally generated parametric 3D face model with a comprehensive library of hand-crafted assets to render training images with corresponding 3D head mesh and 2D facial landmarks. Yet, the dataset consists of only tight face crops and requires manually generating mesh textures, limiting its scalability. Manipulating 2D images can be an alternative to using a 3D graphics pipeline. [76] fit a 3DMM to face images and warp them to augment the head pose. [45] composite hand images onto faces to improve face detection. These approaches can only make minor adjustments to existing images, limiting their use. In contrast, VGGHeads directly samples from a wide distribution of large diffusion models and easily scales to an arbitrary number of train samples and types of scenes.

3. Dataset

Our goal is to create a dataset consisting of image-label pairs, where the label for each image is a set of head bounding boxes and 3D head model parameters. The pipeline generates fully synthetic images using large pre-trained latent diffusion models [48]. We then train a binary head detection model on these synthetic samples and leverage an off-the-shelf 3D head alignment model [43] to predict 3DMM parameters for each generated head.

3.1. Generation Pipeline

The dataset generation process consists of the following stages: (1) images are generated with a latent diffusion model conditioned on a large real-world dataset, (2) a small subset of data is manually labeled with head bounding boxes to train a binary head detector on synthetic data, (3) for each detected head in generated images we predict the 3D head model parameters and (4) the final dataset is automatically filtered to remove extra noise and privacy sensitive samples. The full pipeline is illustrated in Fig. 2.

Image Generation: Latent diffusion models have achieved remarkable progress in high-quality image generation [24, 48]. However, multi-object generation is currently still a challenge [63]. To generalize well to in-the-wild settings, a large-scale dataset of human images should contain various scenes. This includes the ability to model multiple complex backgrounds with different amounts of people and interactions between objects within a scene. To overcome this limitation, we generate images via an intermediate representation: 2D human poses. The pose encodes positions, poses, and scales of human bodies. We condition image

generation on the pose [44], constraining the task, which makes generations much more reliable and offers a degree of control. We predict poses [2] and image descriptions from a subset of the LAION dataset [54] to model a wide variety of real-world scenes. The ground truth image descriptions in the dataset contain much privacy-sensitive information, so instead, we use BLIP-VQA [32] to predict subject-neutral scene descriptions. We demonstrate that this approach allows us to significantly reduce ethnic, gender, and age biases by modifying prompts to ensure sampling from a wider distribution. The T2I-Adapter model [44] injects skeleton feature maps into the decoder blocks of the SDXL [48] model to generate high-resolution synthetic data.

Annotations: Available face detection models [12] are trained to detect only the facial area and are limited to mainly frontal poses; thus, they do not generalize well to a wide range of head angles, which is crucial for many head modeling tasks. In addition, labeling faces on side poses is ambiguous due to occlusions and the absence of clear visual markers. To create consistent labels on synthetic data across *all* pose ranges, we manually label $10,000$ images with head bounding boxes—the smallest axis-parallel rectangles including all visible pixels of the head. While annotating the subset, we manually removed potentially harmful or privacy-sensitive content. The overall annotation process took 56 hours.

In a second stage, we train RT-DETR [42] as a binary head detector on the small set of annotated images to be able to detect heads accurately on the synthetic dataset for future self-labeling. The model achieves **0.925** mAP on a validation subset of 2000 synthetic images.

We employ the trained binary detector to locate and crop all heads in the dataset to generate the final annotations. We represent the human head with a 3D morphable model, FLAME [33]. The FLAME model encodes the 3D head mesh with a small set of disentangled model parameters, effectively combining head shape, expression, and pose. It consists of a set of 5023 vertices, allowing it to be used as a base representation for a variety of downstream tasks. We use the off-the-shelf state-of-the-art FLAME regressor [43] to predict a vector of 413 FLAME parameters for each head crop.

Data Filtering: Despite the high quality of the average generated samples, the latent conditional diffusion model can still fail to generate complex scenes in case of out-of-distribution body poses or pose estimation fail cases. It is crucial to filter out potential wrong generations to decrease the noise level in the dataset and guarantee the strong performance of the models trained on it. We utilize the pre-trained binary head detection model from the previous step to remove noisy samples over several stages: (1) images with no heads detected are removed; (2) we detect the heads on the original and flipped image and remove samples where the number of the detected heads differs; (3) we utilize the fact that the head detector should also detect every face. We predict the face locations on the image with RetinaFace [12] and remove the images where the detected face has no overlap with the detected head bounding boxes; (4) we split the image vertically by half and filter the samples where the total number of detected heads in both crops is not equal to the original image. We found this helpful in removing images with many tiny heads, which might often be deformed due to limited resolution.

3.2. Safety & Privacy

Many datasets have been scraped from the internet without privacy and copyright considerations. Large-scale web datasets may also include harmful content that cannot always be manually detected at scale. Our purely synthetic dataset can largely mitigate these issues and can be efficiently scaled to an arbitrary size.

Content Safety: The latent diffusion models have been trained on billions of images from the internet and thus might be prone to generating harmful or potentially sensitive content. Even though modern generative models use extensive data filtering to exclude such cases, we also include several additional stages of filtering to remove any potential NSFW content produced by the LDM. Initially, because the pipeline can generate numerous images, we remove those with original ground truth labels indicating they contain NSFW or potentially NSFW content. In the generation pipeline, we utilize a CLIP [49] based NSFW filter [1] to flag and remove harmful content. We also add the embeddings of various keywords that might trigger NSFW content generation with a negative weight. As the last step, we classify and filter the generated images with an open-source NSFW classification model [30].

Content Privacy: We investigate whether diffusion models can fully reproduce training samples, potentially leaking personal data. [6] show that a latent diffusion model can memorize some of its training set and reproduce its samples. Stable Diffusion [51] is shown to be the least sensitive to training sample memorization and, in many cases, the algorithm only recovers images similar at the level of scene composition while ignoring finer details. These finer details, however, are crucial to recover a person's identity. Most of the recovered training samples in [6] are photographs of public figures for which there are multiple training samples. Moreover, the associated text also often contains their name. We hypothesize that most of the identifiable visual features of a person are stored within the text encoder and are encoded with the name of a person. To verify this hypothesis, we fine-tuned a Stable Diffusion model [48] on a subset from the RaFD dataset [31]. The dataset contains multiple high-resolution photos of 61 people capturing facial expressions and side poses. To evaluate memorization, we generate

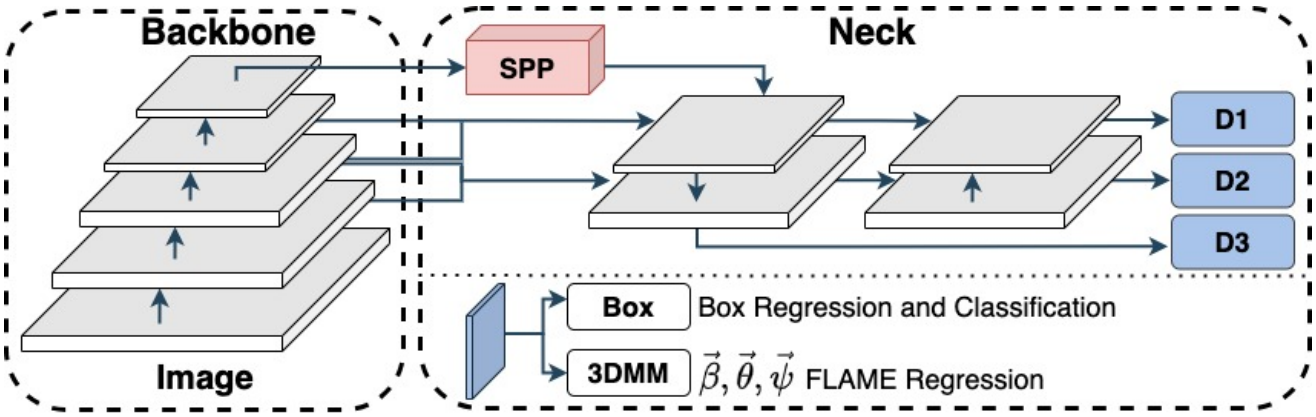

Figure 3. **Model Architecture.** VGGHeads extends YOLO-NAS [2] architecture to predict the 3D Morphable Model parameters along with the head bounding boxes from the multi-scale feature maps.

faces with prompts predicted from the train samples and try to re-identify the generated people in the training dataset. Interestingly, the re-id model [11] fails to identify the people in the original dataset. We observe that the model (a) often mixes the facial features of different people from the original dataset and (b) does not learn to recover finer facial details that can capture a person's identity. However, fine-tuning a second model on a single person results in strong memorization, which hints that large diffusion models might store the identity information of persons given in their names in text. To mitigate this, we employ the GliNER [67] model to automatically detect (first and last) names in the prompt and remove such samples from the dataset. Additionally, we use a simple BLIP model [32] to describe the scene composition, ignoring the ground truth prompt that might contain privacy-sensitive information, such as names. Moreover, as an additional filtering stage, we construct the database of the face embeddings from the Celeb-A [40] and remove all the data samples with faces re-identified in the celebrities database. This approach significantly mitigates privacy concerns, allowing the dataset to be used for a wide range of tasks.

3.3. Dataset Statistics

We sample 1.7 million images from LAION-FACE [72], a subset of LAION [54] dataset that contains images of people. We filter out 20.6% of the data that might contain privacy-sensitive or NSFW content. We only use the human pose prediction and the predicted image description from these images, discarding all visual data. We then generated the 1.3 million synthetic images up to 1280x1280px size. Further data postprocessing removed 19.9% of images with additional NSFW and noise filters. The final dataset consists of $1,022,944$ images with $2,219,146$ heads annotated with bounding boxes and 3D model parameters. The overall generation process took 4000 GPU hours.

4. Method

Our rich ground truth annotations allow us to train a model that estimates a compact 3D head representation of multiple people from an RGB image in a single forward pass. For each head, we predict a vector of 3DMM parameters disentangled into shape, expression, and pose. As every vertex can be mapped to a face part, both head, face and other head parts bounding box can be recovered from the reprojected head mesh. Compared to other methods, this setup encodes a more general representation that serves as a base for other downstream head modeling tasks Tab. 1. The architecture is illustrated in Fig. 3. The model is based on the YOLO-NAS [2] architecture for object detection. The base architecture is extended with six separate modules predicting a human face's shape, expression, jaw, pose, translation, and scale parameters, achieving an extra level of disentanglement.

4.1. Objective Functions

We introduce a multi-component loss function for the end-to-end training of the model to provide supervision for different sets of parameters. The loss function consists of five different parts. Two commonly used loss components optimize the bounding box detection: **Bounding Box Regression Loss** (L_{bbox}) and **Classification Loss** (L_C). Additionally, we extend the objective function with three loss components, each optimizing different properties of the 3D head model. **3D Vertices Loss** measures goodness-of-fit of the 3D Head Shape (L_{3D}), **Rotation Loss** (L_R) optimize the 3D Head Pose and the **Reprojection Loss** (L_{proj}) fit scale and translation. The detailed ablation studies Tab. 7 show the importance of the introduced components.

Reprojection Loss: We measure the discrepancy between the reprojected vertices and ground truth 2D keypoint coordinates. The common approach is to use the L1 norm, which calculates the absolute difference between the pre-

Table 1. **Model Comparison.** Our model recovers a wider head representation space.

Model	Face Box	Head Box	2D Landmarks	3D Landmarks	3D Pose	3D Shape	Expression
PyramidBox [55]	✓	✗	0	0	✗	✗	✗
Img2Pose [3]	✓	✗	0	0	✗	✗	✗
RetinaFace [12]	✓	✗	5	1000	✓	✗	✗
VGGHeads (Ours)	✓	✓	2470	2470	✓	✓	✓

dicted and ground truth keypoints coordinates:

$$L_{\text{reproj}(v_p,v_{gt})} = \frac{1}{N}\sum_{i=1}^{N}\left|v_p^i - v_{\text{gt}}^i\right|$$

where N is the number of keypoints.

3D Vertices Loss: Following DAD-3D [43] we calculate the L2 Loss over the normalized and unrotated 3D Head Vertices. The global rotation predictions are set to zero to evaluate the discrepancy between our predictions and the ground truth in 3D. The 3D vertices are computed from the 3DMM parameters using a differentiable FLAME layer. We subsample the set of vertices by removing ears, eyeballs, and neck parts. The ground truth and the predicted mesh can differ in scale and location, so we normalize both to fit into the unit cube after subsampling.

The final loss term measures the discrepancy between normalized subsampled vertices:

$$L_{3D}(v_p, v_{gt}) = \frac{1}{N}\sum_{i=1}^{N}\left|v_p^i|_{\mathbf{R}=\mathbf{0}} - v_{\text{gt}}^i\right|_2$$

Rotation Loss: The model directly predicts an over-parametrized 6D rotation representation, enabling the minimization of the distance between rotation matrices directly. Instead of using the Frobenius norm, which does not align with the SO(3) manifold geometry, we employ the geodesic distance to measure the shortest path between two 3D rotations. Let R_p and R_{gt} be the estimated and ground truth rotation matrices, respectively, both belonging to SO(3). The geodesic distance between these two rotation matrices is defined as:

$$L_R(R_p, R_{gt}) = cos^{-1}\left(\frac{\text{tr}(R_p R_{gt}^T) - 1}{2}\right)$$

Detection Losses: The focal loss L_c [36], which addresses class imbalance by assigning higher weights to hard-to-classify examples, and Complete Intersection over Union (CIoU) L_{reg} [73], which incorporates IoU, center point distance, and aspect ratio for bounding box regression, are standard components of our detection model

The final loss is calculated as follows: $L = \alpha_{\text{3D}}L_{\text{3D}} + \alpha_{\text{R}}L_{\text{R}} + \alpha_{\text{reproj}}L_{\text{reproj}} + \alpha_{\text{c}}L_{\text{c}} + \alpha_{\text{reg}}L_{\text{reg}}$.

4.2. Implementation Details

We implemented our models using PyTorch. The model is initialized using the pre-trained weights on COCO [34]. The differentiable FLAME layer is kept fixed during the training. The number of learnable head shape and expression parameters are set to 300 and 100, respectively. All the models are trained using **4 RTX A6000** GPU, with a batch size of 80. The training takes 7 days to converge. To preserve the scale ratio and shape of the head, images are padded to the square size and then resized to 640×640. To further reduce the domain gap between the generated and the real-world images, we apply extensive data augmentations such as blurring, noising, compressing, and image manipulating color and image contrast.

5. Experimental Evaluation

We extensively evaluate the dataset and the proposed method on various head-related tasks.

5.1. Head Pose Estimation

We evaluate the accuracy of 3D Head Pose Estimation on AFLW2000-3D [75] and BIWI [15] datasets. The AFLW2000-3D Dataset [75] comprises the first 2,000 subjects from the AFLW dataset, re-annotated to include image-level 68 3D landmarks and detailed pose annotations. The BIWI Dataset [15] was collected in a laboratory environment by recording RGB-D video of various subjects using a Kinect v2 device. It includes frames with head rotations of ±75° for yaw, ±60° for pitch, and ±50° for roll. Each subject's point cloud was fitted with a 3D model, and head rotations were tracked to generate the pose annotations.

Results: We report the results in Tab. 3.VGGHeads outperforms most end-to-end pose prediction methods [3, 12]. VGGHeads achieves superior results to most 3DMM estimators and direct pose regression methods by a large margin and shows comparable performance to other state-of-the-art methods for head pose estimation, even though not being optimized solely for this problem and not using any real images during the training.

Figure 4. **Versatility.** Our model is able to predict many types of head annotations and works across all datasets.

Table 2. **Dataset Evaluation.** The model trained on VGGHeads shows better performance on 3D Head Alignment and Pose Estimation tasks.

Model	Dataset	DAD-3D				AFLW	BIWI	FDDB
		NME↓	Z_5 Accuracy↑	CD↓	Pose Error↓	MAE↓	MAE↓	AP50↑
VGGHeads	WIDER	5.03	0.87	5.83	0.38	9.83	5.17	**96.6**
VGGHeads	VGGHeads	**2.92**	**0.93**	**4.00**	**0.18**	**3.67**	**3.58**	96.1

5.2. 3D Head Alignment

We utilize the DAD-3DHeads Benchmark [43] to evaluate the 3D Dense Head Alignment from an image and robustness to extreme poses. The benchmark consists of 2,746 images annotated with the meshes in FLAME topology and measures the pose fitting, as well as both face and head shape matching. It includes heads in extreme poses, illumination, occlusions, and other challenging cases. As the images might have more than a single head, we extract the head with the highest overlap with the ground truth-bounding box.

Results: VGGHeads significantly outperforms RingNet [53] and 3DDFA-v2 [19], though these methods were trained on real images and optimized to predict the 3D head model from tight crops. We also achieve comparable results to DAD-3D [43] even though this model was trained on the dataset from the same distribution as the benchmark. The results demonstrate that our method can fit pose, head shape, and expression on real images even in challenging conditions.

The non-obvious advantage of FLAME representation for head alignment is that the zero coordinate in FLAME space is located in the geometrical center of the 3D head model. This allows us to implement consistent alignment and normalization of the human head across the wide range of poses so that the center of the "skull" will be always located in the center of the cropped image Fig. 5. In contrast to face alignment methods, it preserves the scale and does not crop parts of the head which is crucial for preprocessing methods of the detailed 3D head modeling tasks.

5.3. Face Detection

The last step is to validate the model's ability to detect heads and faces under different conditions. Though the model was trained to detect head bounding box locations, the 3D representation also encodes face boxes, allowing us to evaluate the approach on Face Detection benchmarks [26, 66]. To compute bounding boxes we calculate minimum bounding rectangle of the subset of face vertices for each detected head and filter out detections where $|\text{yaw}| > \frac{\pi}{2}$, so that the face is not visible. In contrast to other methods, we do not focus on detecting tiny faces in the image since the 3DMM parameters are highly ambiguous in cases where the bounding box area is smaller than the amount of vertices. Still, VGGHeads achieves comparable performance on FDDB [26].

5.4. Ablation Study

We verify the separate components' efficiency for the data generation and model training pipeline.

Data Generation: We test the impact of using larger diffusion models to generate data and different conditioning mechanisms by generating $20,000$ images in each setup. We calculate FID [23] and Inception Score [52] for every setup to measure the generated samples' diversity and realism. The experiment shows that a more advanced diffusion model [48] plays a key role in generating high-quality data, significantly outperforming the analogous setup with Stable Diffusion 1.5 [51]. Additionally, we compare ControlNet [70] to T2I-Adapter [44] as the conditioning module (Tab. 6). While the metrics between the two setups are comparable, ControlNet frequently generates deformed bodies, so we use the T2I-Adapter in the final pipeline.

Model Training: We analyze the performance of our method when removing losses from the training (*cf*. Tab. 7). Removing either loss reduces the performance of our method. We find that adding rich supervision of the normalized 3D vertices locations enables the model to better reconstruct the head shape in 3D, improving the 3D head pose fitting. The geodesic rotation loss provides direct pose supervision and

Table 3. **3D Head Pose Estimation.** VGGHeads achieves state-of-the-art performance comparing to other end-to-end methods on AFLW [75] and BIWI [15] benchmarks.

			AFLW				BIWI			
Model	**End to End**	**3DMM**	**MAE** ↓	**Pitch** ↓	**Roll** ↓	**Yaw** ↓	**MAE** ↓	**Pitch** ↓	**Roll** ↓	**Yaw** ↓
RetinaFace [12]	✓	✗	6.22	9.64	3.92	5.10	4.49	6.42	2.97	4.07
Img2Pose [3]	✓	✗	3.91	5.03	**3.28**	3.43	**3.79**	**3.55**	3.24	4.57
VGGHeads	✓	✓	**3.76**	**4.91**	3.37	**3.00**	**3.79**	5.24	**2.65**	**3.47**

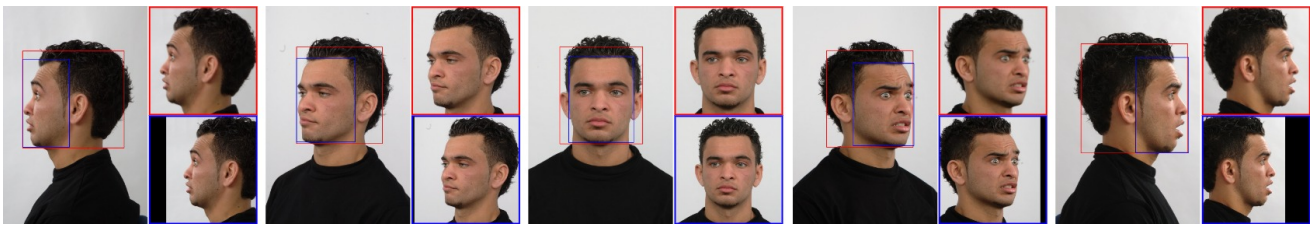

Figure 5. **Head Alignment.** VGGHeads introduce more consistent alignment across various poses by ensuring the center of the head in 3D is reprojected to the center of the aligned image. VGGHeads, RetinaFace [12].

Table 4. **DAD3D-Heads.** VGGHeads achieves superior performance to RingNet and 3DDFA-V2, while being only slightly inferior to the methods that was trained on the benchmark. E2E: end to end.

Model	**E2E**	**NME**↓	Z_5 **Acc.**↑	**Chamf. Dist.**↓	**Pose Err.**↓
3DDFA-V2 [19]	✗	3.580	-	6.170	0.527
RingNet [53]	✗	8.757	0.880	5.166	0.438
DAD-3DNet [43]	✗	2.302	0.954	3.178	0.138
VGGHeads	✓	2.917	0.933	4.002	0.179

Table 5. **Face Detection.** The model trained on VGGHeads data is not optimized for tiny faces detection but with additional finetuning it shows comparable results to state-of-the-art detectors while recovering more complete representation.

Model	**Dataset**	**FDDB**	**WIDER Val (AP50)**		
		AP50↑	**Easy**↑	**Med.**↑	**Hard**↑
RetinaFace [12]	WIDER	96.2	**94.6**	**93.0**	**80.4**
img2pose [3]	WIDER	96.1	86.5	82.9	61.3
VGGHeads	VGGHeads	96.1	56.3	51.0	29.2
VGGHeads	VGGHeads + WIDER	**96.6**	92.6	88.9	70.3

Table 6. **Generators.** We experiment with different image generators [48, 51] and control mechanisms [44, 70]. Our method is not specific to any combination and will further improve with better generators.

Model	**Condition**	**FID**↓	**IS**↑
SD 1.5	ControlNet	7.86	13.59
SDXL	ControlNet	4.18	**15.09**
SDXL	T2I	**3.22**	14.37

Table 7. **Ablation.** Removing any loss reduces the performance on all three datasets.

Model	**VGGHeads Val**			**AFLW**	**FDDB**
	NME↓	**FR**↓	**MAE**↓	**MAE**↓	**AP50**↑
VGGHeads	**1.975**	0.122	**2.470**	**5.03**	**88.5**
w/o L_R	2.052	**0.113**	2.863	6.27	87.9
w/o L_{3D}	2.050	0.128	2.600	5.13	87.9

reduces the 3D head pose error significantly. For computational efficiency the ablation experiments were conducted on a manually labeled subset of the VGGHeads dataset (Sec. 3.1).

6. Conclusion

We have developed and will release a comprehensive dataset for human head detection and 3D mesh estimation, created using diffusion models. It overcomes the limitations of traditional datasets, which often grapple with issues of bias, privacy, and ethical concerns. Additionally, we proposed a novel architecture and model, trained explicitly on this synthetic dataset, capable of accurately reconstructing multiple head meshes from a single image. Our extensive experimental evaluations reveal that models trained with our synthetic data perform exceptionally well on real images, proving the dataset's generalizability and versatility across various applications. Our research demonstrates that synthetic data generated via diffusion models can effectively close the gap

between synthetic and real-world applications, facilitating future progress in 3D head modeling and beyond. Furthermore, the detailed synthetic data generation pipeline we describe can be adapted for other tasks and domains. The dataset, code, and model will be made publicly available, thereby supporting further research and development in the field.

Acknowledgements. We would like to thank Tetiana Martyniuk and Iro Laina for paper proofreading and valuable feedback. We also thank the Armed Forces of Ukraine for providing security to complete this work.

References

[1] Machine vision & learning group lmu. safety checker model card. https://huggingface.co/CompVis/stable-diffusion-safety-checker, 2022. Accessed: 2023-11-16. 4

[2] Shay Aharon, Louis-Dupont, Ofri Masad, Kate Yurkova, Lotem Fridman, Lkdci, Eugene Khvedchenya, Ran Rubin, Natan Bagrov, Borys Tymchenko, Tomer Keren, Alexander Zhilko, and Eran-Deci. Super-gradients, 2021. 3, 4, 5, 12

[3] Vitor Albiero, Xingyu Chen, Xi Yin, Guan Pang, and Tal Hassner. img2pose: Face alignment and detection via 6dof, face pose estimation. In *Proceedings of the IEEE/CVF conference on computer vision and pattern recognition*, pages 7617–7627, 2021. 2, 6, 8, 14

[4] Volker Blanz and Thomas Vetter. A morphable model for the synthesis of 3d faces. In *Conference on Computer graphics and interactive techniques*, pages 187–194, 1999. 2

[5] Yohann Cabon, Naila Murray, and Martin Humenberger. Virtual kitti 2. *arXiv preprint arXiv:2001.10773*, 2020. 3

[6] Nicolas Carlini, Jamie Hayes, Milad Nasr, Matthew Jagielski, Vikash Sehwag, Florian Tramer, Borja Balle, Daphne Ippolito, and Eric Wallace. Extracting training data from diffusion models. In *32nd USENIX Security Symposium (USENIX Security 23)*, pages 5253–5270, 2023. 4

[7] Xiangxiang Chu, Liang Li, and Bo Zhang. Make repvgg greater again: A quantization-aware approach. In *Proceedings of the AAAI Conference on Artificial Intelligence*, pages 11624–11632, 2024. 12

[8] Jifeng Dai, Yi Li, Kaiming He, and Jian Sun. R-fcn: Object detection via region-based fully convolutional networks. *Advances in neural information processing systems*, 29, 2016. 2

[9] Navneet Dalal and Bill Triggs. Histograms of oriented gradients for human detection. In *2005 IEEE computer society conference on computer vision and pattern recognition (CVPR'05)*, pages 886–893. Ieee, 2005. 2

[10] Radek Daněček, Michael J Black, and Timo Bolkart. Emoca: Emotion driven monocular face capture and animation. In *Proceedings of the IEEE/CVF Conference on Computer Vision and Pattern Recognition*, pages 20311–20322, 2022. 2, 12

[11] Jiankang Deng, Jia Guo, Niannan Xue, and Stefanos Zafeiriou. Arcface: Additive angular margin loss for deep face recognition. In *Proceedings of the IEEE/CVF conference on computer vision and pattern recognition*, pages 4690–4699, 2019. 1, 5

[12] Jiankang Deng, Jia Guo, Evangelos Ververas, Irene Kotsia, and Stefanos Zafeiriou. Retinaface: Single-shot multi-level face localisation in the wild. In *Proceedings of the IEEE/CVF conference on computer vision and pattern recognition*, pages 5203–5212, 2020. 2, 4, 6, 8, 14

[13] Bardia Doosti, Shujon Naha, Majid Mirbagheri, and David J. Crandall. Hope-net: A graph-based model for hand-object pose estimation. In *IEEE Conference on Computer Vision and Pattern Recognition (CVPR)*, 2020. 14

[14] Kaiwen Duan, Song Bai, Lingxi Xie, Honggang Qi, Qingming Huang, and Qi Tian. Centernet: Keypoint triplets for object detection. In *Proceedings of the IEEE/CVF international conference on computer vision*, pages 6569–6578, 2019. 12

[15] Gabriele Fanelli, Thibaut Weise, Juergen Gall, and Luc Van Gool. Real time head pose estimation from consumer depth cameras. In *Joint pattern recognition symposium*, pages 101–110. Springer, 2011. 6, 8, 13

[16] Yao Feng, Vasileios Choutas, Timo Bolkart, Dimitrios Tzionas, and Michael J Black. Collaborative regression of expressive bodies using moderation. In *2021 International Conference on 3D Vision (3DV)*, pages 792–804. IEEE, 2021. 3, 12, 13, 14

[17] Yao Feng, Haiwen Feng, Michael J Black, and Timo Bolkart. Learning an animatable detailed 3d face model from in-the-wild images. *ACM Transactions on Graphics (ToG)*, 40(4): 1–13, 2021. 2, 12

[18] Jianzhu Guo, Xiangyu Zhu, and Zhen Lei. 3ddfa. https://github.com/cleardusk/3DDFA, 2018. 2, 14

[19] Jianzhu Guo, Xiangyu Zhu, Yang Yang, Fan Yang, Zhen Lei, and Stan Z Li. Towards fast, accurate and stable 3d dense face alignment. In *European Conference on Computer Vision (ECCV)*, 2020. 2, 7, 8, 12, 14

[20] Yandong Guo, Lei Zhang, Yuxiao Hu, Xiaodong He, and Jianfeng Gao. Ms-celeb-1m: A dataset and benchmark for large-scale face recognition. In *Computer Vision–ECCV 2016: 14th European Conference, Amsterdam, The Netherlands, October 11-14, 2016, Proceedings, Part III 14*, pages 87–102. Springer, 2016. 1

[21] Kaiming He, Xiangyu Zhang, Shaoqing Ren, and Jian Sun. Spatial pyramid pooling in deep convolutional networks for visual recognition. *IEEE transactions on pattern analysis and machine intelligence*, 37(9):1904–1916, 2015. 12

[22] Thorsten Hempel, Ahmed A Abdelrahman, and Ayoub Al-Hamadi. Toward robust and unconstrained full range of rotation head pose estimation. *IEEE Transactions on Image Processing*, 33:2377–2387, 2024. 14

[23] Martin Heusel, Hubert Ramsauer, Thomas Unterthiner, Bernhard Nessler, and Sepp Hochreiter. Gans trained by a two time-scale update rule converge to a local nash equilibrium. *Advances in neural information processing systems*, 30, 2017. 7

[24] Jonathan Ho, Chitwan Saharia, William Chan, David J Fleet, Mohammad Norouzi, and Tim Salimans. Cascaded diffusion models for high fidelity image generation. *The Journal of Machine Learning Research*, 23(1):2249–2281, 2022. 3

[25] Sergey Ioffe and Christian Szegedy. Batch normalization: Accelerating deep network training by reducing internal covariate shift. In *International conference on machine learning*, pages 448–456. pmlr, 2015. 12

[26] Vidit Jain and Erik Learned-Miller. Fddb: A benchmark for face detection in unconstrained settings. Technical report, UMass Amherst technical report, 2010. 7, 13

[27] Peiyuan Jiang, Daji Ergu, Fangyao Liu, Ying Cai, and Bo Ma. A review of yolo algorithm developments. *Procedia computer science*, 199:1066–1073, 2022. 2

[28] Davis E. King. Dlib-ml: A machine learning toolkit. *Journal of Machine Learning Research*, 10:1755–1758, 2009. 14

[29] Orest Kupyn and Christian Rupprecht. Dataset enhancement with instance-level augmentations. *arXiv preprint arXiv:2406.08249*, 2024. 3

[30] Gant Laborde. Deep nn for nsfw detection. 4

[31] Oliver Langner, Ron Dotsch, Gijsbert Bijlstra, Daniel HJ Wigboldus, Skyler T Hawk, and AD Van Knippenberg. Presentation and validation of the radboud faces database. *Cognition and emotion*, 24(8):1377–1388, 2010. 4, 12

[32] Junnan Li, Dongxu Li, Caiming Xiong, and Steven Hoi. Blip: Bootstrapping language-image pre-training for unified vision-language understanding and generation. In *International Conference on Machine Learning*, pages 12888–12900. PMLR, 2022. 3, 4, 5

[33] Tianye Li, Timo Bolkart, Michael J. Black, Hao Li, and Javier Romero. Learning a model of facial shape and expression from 4d scans. *ACM Trans. Graph.*, 36(6), 2017. 2, 4

[34] Tsung-Yi Lin, Michael Maire, Serge Belongie, James Hays, Pietro Perona, Deva Ramanan, Piotr Dollár, and C Lawrence Zitnick. Microsoft coco: Common objects in context. In *Computer Vision–ECCV 2014: 13th European Conference, Zurich, Switzerland, September 6-12, 2014, Proceedings, Part V 13*, pages 740–755. Springer, 2014. 6

[35] Tsung-Yi Lin, Piotr Dollár, Ross Girshick, Kaiming He, Bharath Hariharan, and Serge Belongie. Feature pyramid networks for object detection. In *Proceedings of the IEEE conference on computer vision and pattern recognition*, pages 2117–2125, 2017. 12

[36] Tsung-Yi Lin, Priya Goyal, Ross Girshick, Kaiming He, and Piotr Dollár. Focal loss for dense object detection. In *Proceedings of the IEEE international conference on computer vision*, pages 2980–2988, 2017. 6

[37] Tsung-Yi Lin, Priya Goyal, Ross Girshick, Kaiming He, and Piotr Dollár. Focal loss for dense object detection. In *Proceedings of the IEEE international conference on computer vision*, pages 2980–2988, 2017. 2

[38] Feng Liu, Luan Tran, and Xiaoming Liu. 3d face modeling from diverse raw scan data. In *Proceedings of the IEEE/CVF international conference on computer vision*, pages 9408–9418, 2019. 12, 14

[39] Shu Liu, Lu Qi, Haifang Qin, Jianping Shi, and Jiaya Jia. Path aggregation network for instance segmentation. In *Proceedings of the IEEE conference on computer vision and pattern recognition*, pages 8759–8768, 2018. 12

[40] Ziwei Liu, Ping Luo, Xiaogang Wang, and Xiaoou Tang. Large-scale celebfaces attributes (celeba) dataset. *Retrieved August*, 15(2018):11, 2018. 5, 12, 13

[41] Ze Liu, Yutong Lin, Yue Cao, Han Hu, Yixuan Wei, Zheng Zhang, Stephen Lin, and Baining Guo. Swin transformer: Hierarchical vision transformer using shifted windows. In *Proceedings of the IEEE/CVF international conference on computer vision*, pages 10012–10022, 2021. 12

[42] Wenyu Lv, Shangliang Xu, Yian Zhao, Guanzhong Wang, Jinman Wei, Cheng Cui, Yuning Du, Qingqing Dang, and Yi Liu. Detrs beat yolos on real-time object detection. *arXiv preprint arXiv:2304.08069*, 2023. 4

[43] Tetiana Martyniuk, Orest Kupyn, Yana Kurlyak, Igor Krashenyi, Jiři Matas, and Viktoriia Sharmanska. Dad-3dheads: A large-scale dense, accurate and diverse dataset for 3d head alignment from a single image. In *Proceedings of the IEEE/CVF Conference on computer vision and pattern recognition*, pages 20942–20952, 2022. 2, 3, 4, 6, 7, 8, 12, 13, 14

[44] Chong Mou, Xintao Wang, Liangbin Xie, Jian Zhang, Zhongang Qi, Ying Shan, and Xiaohu Qie. T2i-adapter: Learning adapters to dig out more controllable ability for text-to-image diffusion models. *arXiv preprint arXiv:2302.08453*, 2023. 4, 7, 8

[45] Behnaz Nojavanasghari, Charles E Hughes, Tadas Baltrušaitis, and Louis-Philippe Morency. Hand2face: Automatic synthesis and recognition of hand over face occlusions. In *2017 Seventh International Conference on Affective Computing and Intelligent Interaction (ACII)*, pages 209–215. IEEE, 2017. 3

[46] Pascal Paysan, Reinhard Knothe, Brian Amberg, Sami Romdhani, and Thomas Vetter. A 3d face model for pose and illumination invariant face recognition. In *IEEE International Conference on Advanced Video and Signal Based Surveillance*, pages 296–301, 2009. 2

[47] Dezhi Peng, Zikai Sun, Zirong Chen, Zirui Cai, Lele Xie, and Lianwen Jin. Detecting heads using feature refine net and cascaded multi-scale architecture. *arXiv preprint arXiv:1803.09256*, 2018. 2

[48] Dustin Podell, Zion English, Kyle Lacey, Andreas Blattmann, Tim Dockhorn, Jonas Müller, Joe Penna, and Robin Rombach. Sdxl: Improving latent diffusion models for high-resolution image synthesis. *arXiv preprint arXiv:2307.01952*, 2023. 3, 4, 7, 8, 13

[49] Alec Radford, Jong Wook Kim, Chris Hallacy, Aditya Ramesh, Gabriel Goh, Sandhini Agarwal, Girish Sastry, Amanda Askell, Pamela Mishkin, Jack Clark, et al. Learning transferable visual models from natural language supervision. In *International conference on machine learning*, pages 8748–8763. PMLR, 2021. 4

[50] Shaoqing Ren, Kaiming He, Ross Girshick, and Jian Sun. Faster r-cnn: Towards real-time object detection with region proposal networks. *Advances in neural information processing systems*, 28, 2015. 2

[51] Robin Rombach, Andreas Blattmann, Dominik Lorenz, Patrick Esser, and Björn Ommer. High-resolution image synthesis with latent diffusion models. In *Proceedings of the IEEE/CVF conference on computer vision and pattern recognition*, pages 10684–10695, 2022. 4, 7, 8

[52] Tim Salimans, Ian Goodfellow, Wojciech Zaremba, Vicki Cheung, Alec Radford, and Xi Chen. Improved techniques

for training gans. *Advances in neural information processing systems*, 29, 2016. 7

[53] Soubhik Sanyal, Timo Bolkart, Haiwen Feng, and Michael J Black. Learning to regress 3d face shape and expression from an image without 3d supervision. In *IEEE Conference on Computer Vision and Pattern Recognition (CVPR)*, pages 7763–7772, 2019. 2, 7, 8, 12, 14

[54] Christoph Schuhmann, Romain Beaumont, Richard Vencu, Cade Gordon, Ross Wightman, Mehdi Cherti, Theo Coombes, Aarush Katta, Clayton Mullis, Mitchell Wortsman, et al. Laion-5b: An open large-scale dataset for training next generation image-text models. *Advances in Neural Information Processing Systems*, 35:25278–25294, 2022. 4, 5

[55] Xu Tang, Daniel K Du, Zeqiang He, and Jingtuo Liu. Pyramidbox: A context-assisted single shot face detector. In *Proceedings of the European conference on computer vision (ECCV)*, pages 797–813, 2018. 2, 6

[56] Roberto Valle, José M Buenaposada, and Luis Baumela. Multi-task head pose estimation in-the-wild. *IEEE Transactions on Pattern Analysis and Machine Intelligence*, 43(8): 2874–2881, 2020. 14

[57] Paul Viola and Michael J Jones. Robust real-time face detection. *International journal of computer vision*, 57:137–154, 2004. 2

[58] Tuan-Hung Vu, Anton Osokin, and Ivan Laptev. Context-aware cnns for person head detection. In *Proceedings of the IEEE International Conference on Computer Vision*, pages 2893–2901, 2015. 2

[59] Yitong Wang, Xing Ji, Zheng Zhou, Hao Wang, and Zhifeng Li. Detecting faces using region-based fully convolutional networks. *arXiv preprint arXiv:1709.05256*, 2017. 2

[60] Erroll Wood, Tadas Baltrušaitis, Charlie Hewitt, Sebastian Dziadzio, Thomas J Cashman, and Jamie Shotton. Fake it till you make it: face analysis in the wild using synthetic data alone. In *Proceedings of the IEEE/CVF international conference on computer vision*, pages 3681–3691, 2021. 3

[61] Cho-Ying Wu, Qiangeng Xu, and Ulrich Neumann. Synergy between 3dmm and 3d landmarks for accurate 3d facial geometry. *arXiv preprint arXiv:2110.09772*, 2021. 14

[62] Weijia Wu, Yuzhong Zhao, Hao Chen, Yuchao Gu, Rui Zhao, Yefei He, Hong Zhou, Mike Zheng Shou, and Chunhua Shen. Datasetdm: Synthesizing data with perception annotations using diffusion models. *arXiv preprint arXiv:2308.06160*, 2023. 3

[63] Weijia Wu, Yuzhong Zhao, Mike Zheng Shou, Hong Zhou, and Chunhua Shen. Diffumask: Synthesizing images with pixel-level annotations for semantic segmentation using diffusion models. *arXiv preprint arXiv:2303.11681*, 2023. 3

[64] Zhenyu Wu, Lin Wang, Wei Wang, Tengfei Shi, Chenglizhao Chen, Aimin Hao, and Shuo Li. Synthetic data supervised salient object detection. In *Proceedings of the 30th ACM International Conference on Multimedia*, pages 5557–5565, 2022. 3

[65] Yuelang Xu, Benwang Chen, Zhe Li, Hongwen Zhang, Lizhen Wang, Zerong Zheng, and Yebin Liu. Gaussian head avatar: Ultra high-fidelity head avatar via dynamic gaussians. *arXiv preprint arXiv:2312.03029*, 2023. 1

[66] Shuo Yang, Ping Luo, Chen-Change Loy, and Xiaoou Tang. Wider face: A face detection benchmark. In *Proceedings of the IEEE conference on computer vision and pattern recognition*, pages 5525–5533, 2016. 7, 13, 15

[67] Urchade Zaratiana, Nadi Tomeh, Pierre Holat, and Thierry Charnois. Gliner: Generalist model for named entity recognition using bidirectional transformer, 2023. 5

[68] Changzheng Zhang, Xiang Xu, and Dandan Tu. Face detection using improved faster rcnn. *arXiv preprint arXiv:1802.02142*, 2018. 2

[69] Hongwen Zhang, Yating Tian, Yuxiang Zhang, Mengcheng Li, Liang An, Zhenan Sun, and Yebin Liu. Pymaf-x: Towards well-aligned full-body model regression from monocular images. *IEEE Transactions on Pattern Analysis and Machine Intelligence*, 45(10):12287–12303, 2023. 3, 12

[70] Lvmin Zhang, Anyi Rao, and Maneesh Agrawala. Adding conditional control to text-to-image diffusion models. In *Proceedings of the IEEE/CVF International Conference on Computer Vision*, pages 3836–3847, 2023. 7, 8, 13

[71] Shifeng Zhang, Xiangyu Zhu, Zhen Lei, Hailin Shi, Xiaobo Wang, and Stan Z Li. S3fd: Single shot scale-invariant face detector. In *Proceedings of the IEEE international conference on computer vision*, pages 192–201, 2017. 2

[72] Yinglin Zheng, Hao Yang, Ting Zhang, Jianmin Bao, Dongdong Chen, Yangyu Huang, Lu Yuan, Dong Chen, Ming Zeng, and Fang Wen. General facial representation learning in a visual-linguistic manner. In *Proceedings of the IEEE/CVF Conference on Computer Vision and Pattern Recognition*, pages 18697–18709, 2022. 5

[73] Zhaohui Zheng, Ping Wang, Wei Liu, Jinze Li, Rongguang Ye, and Dongwei Ren. Distance-iou loss: Faster and better learning for bounding box regression. In *Proceedings of the AAAI Conference on Artificial Intelligence*, pages 12993–13000, 2020. 6

[74] Yijun Zhou and James Gregson. Whenet: Real-time fine-grained estimation for wide range head pose. *arXiv preprint arXiv:2005.10353*, 2020. 14

[75] Xiangyu Zhu, Zhen Lei, Xiaoming Liu, Hailin Shi, and Stan Z Li. Face alignment across large poses: A 3d solution. In *IEEE Conference on Computer Vision and Pattern Recognition (CVPR)*, pages 146–155, 2016. 6, 8, 13

[76] Xiangyu Zhu, Zhen Lei, Xiaoming Liu, Hailin Shi, and Stan Z Li. Face alignment across large poses: A 3d solution. In *Proceedings of the IEEE conference on computer vision and pattern recognition*, pages 146–155, 2016. 1, 3, 13

[77] Wojciech Zielonka, Timo Bolkart, and Justus Thies. Towards metrical reconstruction of human faces. In *European conference on computer vision*, pages 250–269. Springer, 2022. 2, 12

A. Re-Identification on Synthetic Data

Figure 6 provides visual examples of generated samples that were matched with public figures from Celeb-A [40] dataset. Even though the data generation include the prompt anonymization, some parts of the prompts, such as the movie name still might encode identity of famous people. Identifying and removing such samples improve the privacy aspect. Fig. 7 shows an example of an image generated by diffusion model that was finetuned on RaFD [31] dataset, and 2 nearest neighbors from the dataset it was trained on. Even though the model learns features from the original images, in most cases it does combine features from multiple people and fails to recover finer details that encode the identity.

B. Model Details

The architecture is inspired by object detection methods like CenterNet [14] or YOLO-NAS-Pose [2], enabling efficient end-to-end learning. The model is based on the YOLO-NAS [2] architecture for object detection. YOLO-NAS use a neural architecture search engine to enhance the YOLO family of models by optimzing the sizes and structures of stages, block types, the number of blocks, and the number of channels in each stage. We employ the YOLO-NAS-L backbone, though the model is agnostic to the choice of encoder. The "neck" is used to fuse the features generated by the backbone. The visual features from the encoder maps neck are fused by the Spatial Pyramid Pooling [21] module at different scales and processed by Feature Pyramid Network [35] to generate features at different semantic levels. Similarly to other YOLO models, we adopt an anchor-based multi-scale detection scheme. Path Aggregation Network (PAN) [39] transfers positioning features bottom-up. We combine them with the features from FPN to obtain a better feature fusion effect and then directly use the multi-scale fusion feature maps in the PAN for detection. Thus, the detection heads predict bounding boxes and 3DMM parameters on different scales, ensuring high accuracy on different object sizes. This approach allows us to optimize FLAME parameters only on positive anchors, improving training efficiency. It also offers flexibility for applications that may not require full 3D meshes, allowing the extraction of bounding boxes in real time without computing full 3D mesh. The detection head in the YOLO-NAS model predicts the offset of the bounding box position and the scaling of the height and width, as well as the confidence of the prediction. We extend the detection head to also predict the 3DMM parameters by introducing six separate 3D parameter prediction modules, each consisting of two RepVGG blocks [7] and a final 1×1 convolution that predicts the final set of parameters. Each RepVGG block consists of three branches: a 3×3 Convolution followed by BatchNorm [25], a branch of a 1x1 Convolution with bias and a residual branch. Predicting different 3DDM parameters components separately achieves an extra level of disentanglement.

Table 8. **Model Architecture Comparison.** Analysis of different VGGHeads variants in terms of parameters, computational cost, and speed.

Model	Total Parameters	FLOPs (B)	FPS
VGGHeads-L	50,442,706	83.51	60.13
VGGHeads-M	32,378,236	52.01	69.38
VGGHeads-S	17,004,954	22.92	72.34

The weights of the loss components are set to $\alpha_1 = 50, \alpha_2 = 1, \alpha_3 = 1, \alpha_4 = 0.5, \alpha_5 = 2.5$ in the final version.

The framework is agnostic to the choice of backbone and can be adapted to use larger transformer models [41]. Yet, we observe the string performance on a smaller fully convolutional models and stick to this design to allow for real-time multi head mesh recovery. Furthermore the versatility of backbones allow to train even smaller models suitable for wide range of tasks and applications.

C. Head Pose Estimation

The full results on AFLW and BIWI datasets are presented in Tab. 9, Tab. 10. VGGHeads outperforms most of method optimized solely for 3D Head Pose Estimation even though it does not operate on tight head crops.

D. 3D Face Reconstruction

VGGHeads is more coarse than 3D reconstruction methods so detailed 3D face reconstruction is not the goal of our method and a standalone task in itself. Nonetheless, we evaluate the model on the Feng et al. benchmark [38]. The model achieves comparable results to other coarse 3D face reconstruction methods [19, 43, 53] despite not being optimized for shape and expression disentanglement. This performance is surprising since our method predicts the 3D face from a full image, not a tight crop as is typical for this task. While our method aims at solving a different task, it achieves good performance. Moreover, the VGGHeads dataset and model can be complementary to detailed face reconstruction methods such as DECA [17], MICA [77] or EMOCA [10], which often need to be initialized with a crop or initial coarse face shape.

E. Full Body Mesh Recovery

Our approach proves the viability of using synthetic data from diffusion models for body modeling, paving the way for future fully synthetic all-in-one methods. VGGHeads is the first step towards this goal. While full-body reconstruction methods [16, 69], achieved significant progress and attention, they often still rely on upstream face predictors and lack

Figure 6. **Re-ID on Celeb-A.** We automatically detect and removed samples where face in the generated image is matched with one of the faces from Celeb-A dataset [40].

Figure 7. **Preserving Identity.** With subject neutral prompts diffusion Model blends feature of different people from the set it was trained on.

robustness in edge cases. To validate it we evaluate PIXIE's [16] performance on the BIWI [15] dataset for 3D Head Pose.

F. Controllable Generation

Conditioning the image generation on full head mesh helps to preserve the head shape and expression which is crucial for many AR applications. We trained the ControlNet [70] for SDXL [48] model that is conditioned on meshes recovered by our model. The meshes are rendered by mapping to RGB space with Projected Normalized Coordinate Code (PNCC) [76], with the 3D coordinate of each vertex of the normalized head mesh encoded as RGB (NCCx = R, NCCy = G, NCCz = B). The heads on the generated images preserve the pose, expression and shape of the original photo Fig. 10.

G. Qualitative Results

Additional data samples from VGGHeads dataset are presented in Fig. 9.

We also include more visual results on AFLW [75] Fig. 12, BIWI [15] Fig. 13, DAD-3D [43] Fig. 14, WIDER [66] Fig. 8 and FDDB [26] benchmarks Fig. 11.

H. Limitations and Broader Impact

The dataset annotations are based on DAD-3D [43] so we don't aim to model neck, ears and eyeball vertices that are a part of the FLAME topology. The generation pipeline still can produce deformed small faces due to the limited resolution so we don't label and predict the 3D model parameters of the tiny faces. Also, the more advanced filtering methods and nsfw detection methods are a suitable venue for future explorations as on the large scale it is not feasible to guarantee the absolute correctness of the generated samples, even by adding the human evaluation into the process. By

Table 9. AFLW

Model	End to End	3DMM	MAE ↓	Pitch MAE ↓	Roll MAE ↓	Yaw MAE ↓
Dlib [28]	✗	✗	13.29	12.60	9.00	18.27
HopeNet [13]	✗	✗	6.16	6.56	5.44	6.47
6DRepNet [22]	✗	✗	3.61	4.58	2.98	3.27
RingNet [53]	✗	✓	8.27	4.39	13.51	6.92
3DDFA-V2 [19]	✗	✓	7.56	8.48	9.89	4.30
3DDFA [18]	✗	✓	7.39	8.53	7.39	5.40
DAD-3DHeads [43]	✗	✓	3.66	4.76	3.15	3.08
SynergyNet [61]	✗	✓	**3.35**	**4.09**	**2.55**	3.42
RetinaFace [12]	✓	✗	6.22	9.64	3.92	5.10
Img2Pose [3]	✓	✗	3.91	5.03	**3.28**	3.43
VGGHeads	✓	✓	**3.76**	**4.91**	3.37	**3.00**

Table 10. BIWI

Model	End to End	3DMM	MAE ↓	Pitch MAE ↓	Roll MAE ↓	Yaw MAE ↓
Dlib (68 points) [28]	✗	✗	12.25	13.80	6.19	16.76
HopeNet [13]	✗	✗	4.90	6.61	3.27	4.81
WHENet [74]	✗	✗	3.81	4.39	3.06	3.99
6DRepNet [22]	✗	✗	3.78	5.32	2.78	**3.23**
MNN [56]	✗	✗	**3.66**	4.61	**2.39**	3.98
3DDFA [18]	✗	✓	19.07	12.25	8.78	36.18
3DDFA-V2 [19]	✗	✓	8.81	12.08	7.54	6.80
RingNet [53]	✗	✓	7.34	5.37	7.82	8.82
DAD-3DNet [43]	✗	✓	3.98	5.24	2.92	3.79
RetinaFace [12]	✓	✗	4.49	6.42	2.97	4.07
Img2Pose [3]	✓	✗	**3.79**	**3.55**	3.24	4.57
VGGHeads	✓	✓	**3.79**	5.24	**2.65**	**3.47**

Model	3DRMSE↓	Median(mm)↓		Mean(mm)↓		Std(mm)↓	
		HQ	LQ	HQ	LQ	HQ	LQ
3DDFA-V2[19]	2.998	1.500	1.779	1.942	2.350	1.704	2.149
RingNet[53]	2.809	1.698	1.634	2.161	2.113	1.832	1.831
DAD-3DNet [43]	2.749	1.558	1.624	1.940	2.082	1.581	1.795
VGGHeads	2.996	1.622	1.801	2.079	2.353	1.801	2.054

Table 11. **Feng et al.[38]**

Table 12. **Comparison with Full Body Reconstruction [16].** VGGHeads achieves superior performance to full body recovery method [16] on BIWI 3D Head Pose Estimation. This shows that all in one methods still fail on challenging head understanding benchmarks.

Model	MAE↓	Pitch MAE↓	Roll MAE↓	Yaw MAE↓
PIXIE [16]	10.97	16.80	6.19	9.93
VGGHeads	**3.79**	**5.24**	**2.65**	**3.47**

leveraging synthetic data generated through diffusion models, we reduce the privacy, ethics, and safety issues in human subject research, as no real personal data is used so that privacy and ethical standards are upheld. Furthermore, the synthetic dataset's high resolution and detailed annotations provide a robust and versatile resource for developing and testing new models. This approach not only enhances the generalizability and accuracy of models trained on this data but also promotes ethical research practices by eliminating the need for real human subjects. The ability to generate large-scale synthetic datasets paves the way for safer and more inclusive research, free from the constraints and risks associated with real-world data collection. Thus, our work promotes ethical AI practices and sets a standard for future research in this area.

I. Fail Cases

The dataset fail cases are presented in Fig. 15. Typical failure cases are head detector failure (both FP and FN), misaligned mesh on out-of-distribution shapes and poses, severe occlusions, and deformed tiny faces in crowded scenes.

Figure 8. **Qualitative Evaluation.** VGGHeads is able to accurately recover 3D head models on various complex scenes from WIDER Face [66] dataset.

Figure 9. **Dataset Examples.** The synthetic data generation pipeline generates complex realistic real world scenes with multiple objects, covering wide range of poses and backgrounds while reducing age, gender and ethnical biases present in small real world datasets.

Figure 10. **ControlNet with VGGHeads.** The 3D condition provides a strong degree of control for the generative model, preserving shape, pose and expression of the input image.

Figure 11. **Qualitative Evaluation on FDDB.**

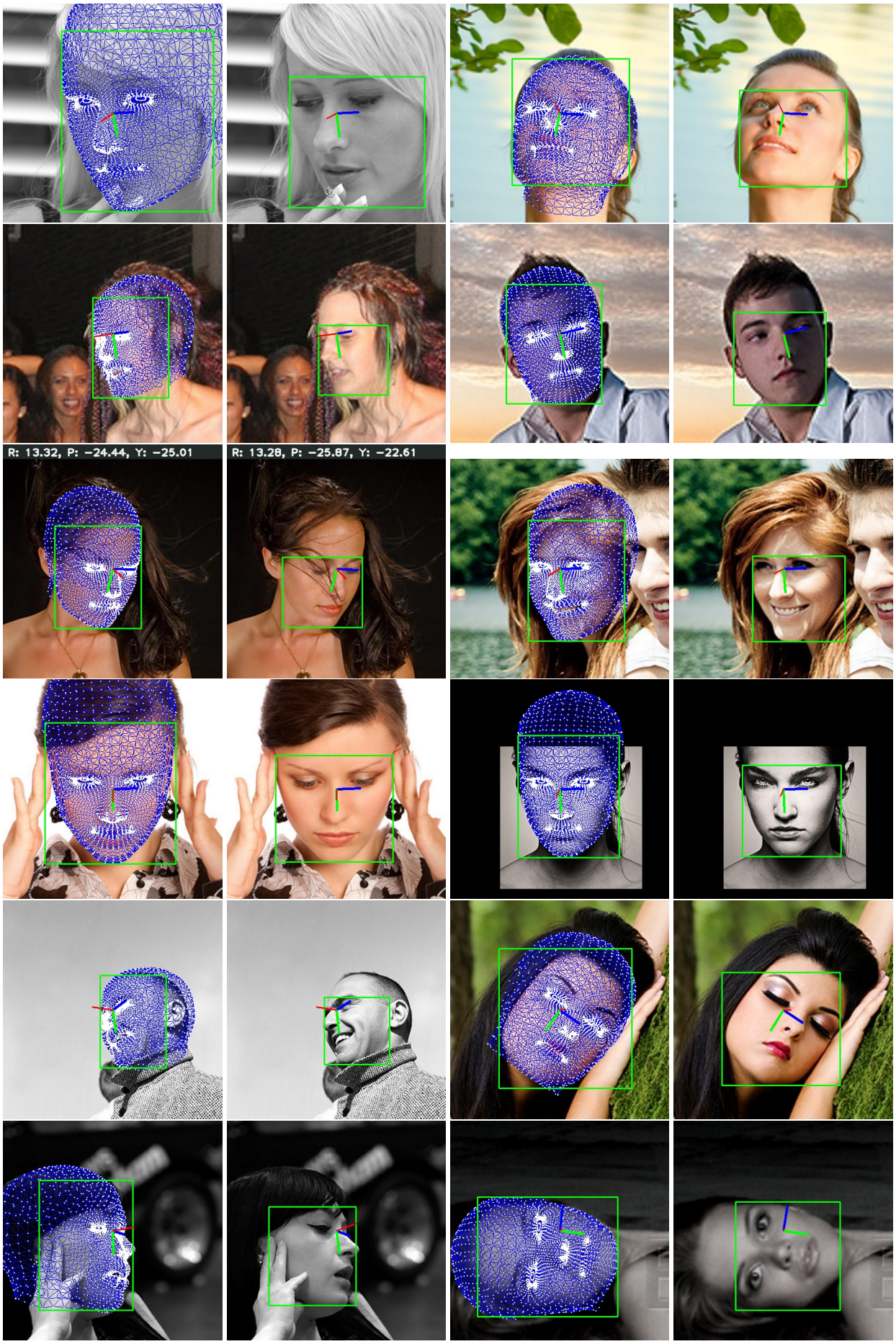

Figure 12. **Qualitative Evaluation on AFLW.**

Figure 13. **Qualitative Evaluation on BIWI.**

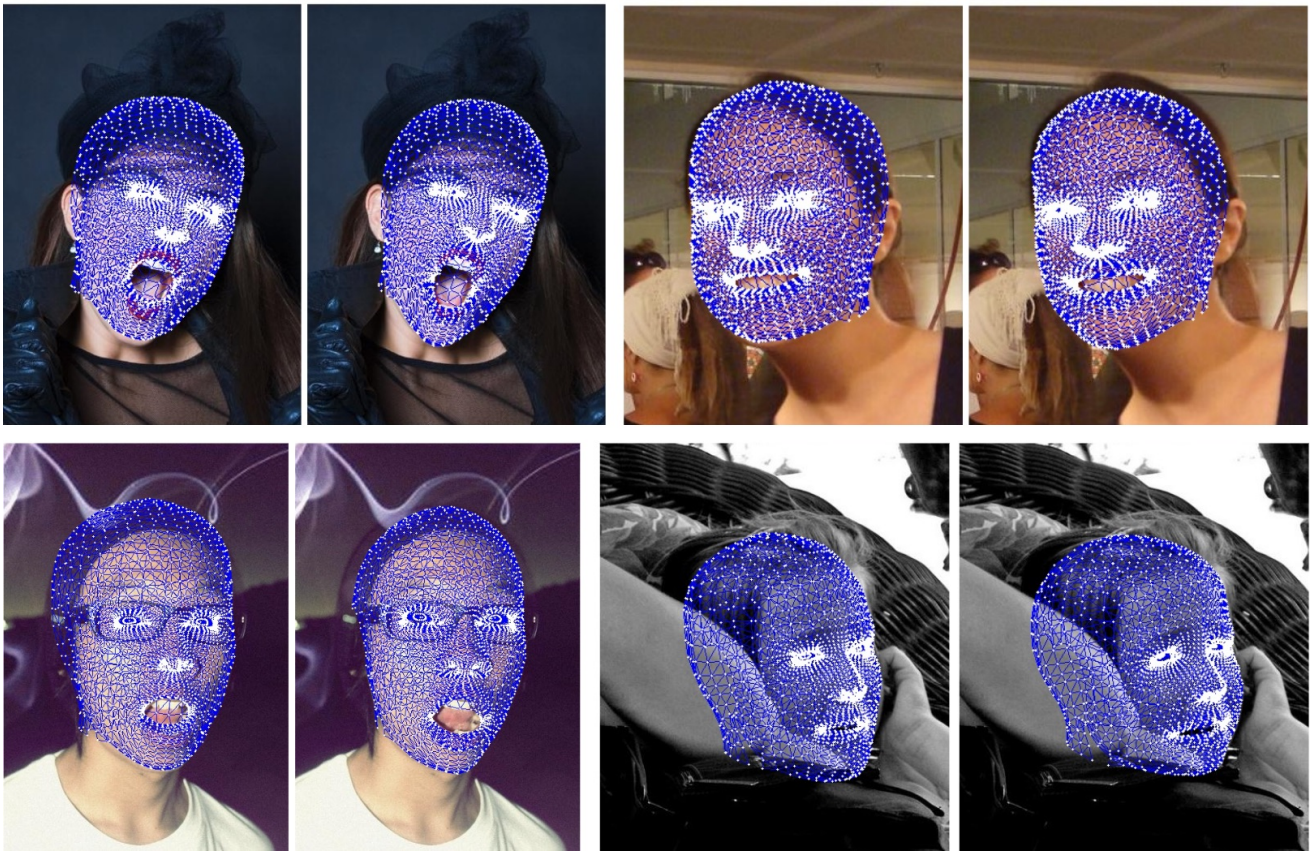

Figure 14. **Qualitative Evaluation on DAD-3D**

Figure 15. **VGGHeads Dataset Fail Cases**